ORIGINAL ARTICLE-CLINICAL SCIENCE

Clinical & Experimental Ophthalmology — WILEY

Automated quantification of uveitic keratic precipitates by use of anterior segment optical coherence tomography

Francesco Pichi MD[1,2] | Giovanni Ometto PhD[3,4] | Alessandro Invernizzi MD[5,6] | Steven Hay COT[1] | Hannah Chaudhry[1] | Shaikha Aljneibi MD[1] | Giovanni Montesano MD[3,4] | Federico Zicarelli MD[5] | Piergiorgio Neri MD, PhD[1,2]

[1]Eye Institute, Cleveland Clinic Abu Dhabi, Abu Dhabi, United Arab Emirates

[2]Cleveland Clinic Lerner College of Medicine, Case Western Reserve University, Cleveland, Ohio, USA

[3]Optometry and Visual Sciences, City University of London, London, UK

[4]NIHR Biomedical Research Centre, Moorfields Eye Hospital NHS Foundation Trust and UCL Institute of Ophthalmology, London, UK

[5]Eye Clinic, Department of Biomedical and Clinical Science "Luigi Sacco," Luigi Sacco Hospital, University of Milan, Milan, Italy

[6]Discipline of Ophthalmology, Sydney Medical School, The University of Sydney, Save Sight Institute, Sydney, New South Wales, Australia

Correspondence
Francesco Pichi, Eye Institute, Cleveland Clinic Abu Dhabi, Al Maryah Island, PO Box 112412, Abu Dhabi, United Arab Emirates.
Email: ilmiticopicchio@gmail.com

Abstract

Background: Evaluation of ocular inflammation via common imaging modalities like optical coherence tomography (OCT) has emphasised cell visualisation, but automated detection of uveitic keratic precipitates (KPs) remains unexplored.

Methods: Anterior segment (AS)-OCT dense volumes of the corneas of patients with uveitic KPs were collected at three timepoints: with active (T0), clinically improving (T1), and resolved (T2) inflammation. At each visit, visual acuity and clinical grading of the anterior chamber cells were assessed. A bespoke algorithm was used to create an en face rendering of the KPs and to calculate their volume and a ratio of the volume of precipitates over the analysed area. The variation of AS-OCT-derived measurements over time was assessed, and compared with clinical grading.

Results: Twenty eyes from 20 patients (13 females, mean age 39 years) were studied. At T0, the mean volume of the corneal KPs was 0.1727 mm^3, and it significantly reduced to 0.1111 mm^3 ($p = 0.03$) only at T2. The ratio between the volume of the KPs and the corneal area decreased from T0 (0.007) to T1 (0.006; $p = 0.2$) and T2 (0.004; $p = 0.009$). There was a statistically significant correlation between the AC cell count and the AS-OCT volume measurements of the KPs at the three time points.

Conclusions: AS-OCT can image uveitic KPs and through a bespoke algorithm we were able to create an en face rendering allowing us to extrapolate their volume. We found that objective quantification of KPs correlated with inflammatory cell counts in the anterior chamber.

KEYWORDS
anterior segment optical coherence tomography, automated algorithm, keratic precipitates

1 | INTRODUCTION

Keratic precipitates (KPs) are collections of inflammatory cells, including polymorphonuclear cells, lymphocytes, and epithelioid cells. These cells are deposited on the corneal endothelium by the aqueous humour in various forms of uveitis,[1] as well as in cases of infectious keratitis and cornea transplant rejection.[2]

In 2005, the SUN working group classified KPs into granulomatous and non-granulomatous types based on their appearance during clinical examination.[3] However, it should be noted that the term 'granulomatous' is not entirely accurate in describing KPs clinically, as it is a histopathological term.[4] Despite this discrepancy, the terminology has been adopted to describe the appearance of KPs under a slit lamp, aiming to provide diagnostic information.

The morphology of KPs can provide clues about the underlying cause of uveitis. For instance, the presence of granulomatous KPs may prompt further investigation into diseases such as tuberculosis, sarcoidosis, Vogt-Koyanagi-Harada syndrome, and syphilis.[5] On the other hand, non-granulomatous KPs are associated with Behçet disease, tubulointerstitial nephritis, uveitis syndrome, or HLAB27-related illnesses.[6] It is worth noting that both types of KPs can coexist or even change over the course of uveitis or be influenced by treatment. Consequently, KPs are considered a secondary result of inflammation and have had limited utility in the diagnosis and treatment of intraocular inflammation.

Given the advancements in imaging techniques like optical coherence tomography (OCT) and artificial intelligence, exploring alternative quantitative methods for analysing KPs seems promising.

Anterior segment OCT (AS-OCT), which was first developed in 1994,[7] is a tool used to assess the cornea, anterior chamber, and KPs in terms of their quantity, location, and characteristics.[8] AS-OCT has been employed in uveitis research to visualise inflammatory cells and flare in the anterior chamber,[9,10] measure iris thickness in specific pathologies like Fuchs Uveitis Syndrome,[11,12] and provide morphological descriptions of KPs.[13] However, further improvements are needed to automate the analysis of KPs using AS-OCT.

In this study, we utilised AS-OCT scans to automatically generate an en face map of KPs and measure their volume. We also investigated the relationship between KPs and other anterior segment parameters.

2 | METHODS

Consecutive patients presenting at the Eye Institute, Cleveland Clinic Abu Dhabi, Abu Dhabi, United Arab Emirates, and at the Eye Clinic, Luigi Sacco Hospital, University of Milan, from 1 August 2022, to 1 February 2023, with a diagnosis of uveitis and noted to have KPs on clinical slit lamp examination were enrolled in this prospective study. The respective coauthors determined Institutional Review Board approval according to the requirements established by their institutional centres (IRB approval #A-2022-042). The study complied with the Health Insurance Portability and Accountability Act of 1996 and followed the tenets of the Declaration of Helsinki. Written informed consent was obtained from all the enrolled subjects.

2.1 | Study subjects

Participants were approached consecutively on attendance at the two uveitis clinics, based on the following inclusion criteria: (1) age ≥18 years; (2) presence of KPs associated with anterior uveitis or panuveitis, either infectious or non-infectious. Patients with a previous diagnosis of corneal ectasia or known for corneal disease were excluded from the study. Patients that met inclusion criteria were assessed at three-time points: active uveitis (T0) with evidence of anterior chamber cells with/without vitritis and evidence of posterior segment inflammation; resolving uveitis (T1) with clinical reduction of the signs of inflammation compared to T0 in response to treatment; quiet eye (T2) with no clinical evidence of intraocular inflammation.

The reference standard test was a routine undilated clinical assessment within a darkened room, carried out by the senior uveitis specialists (FP and AI) with a slit lamp (Haag Streit BM 900 site 1, BQ 900 site 2). The SUN anterior chamber grading was used to assess inflammation (0, no cells seen within a central 1×1 mm long beam; $+0.5$, 1–5 cells seen within the shaft;$+1$, 6–15;$+2$, 16–25; $+3$, 26–50;$+4$, more than 51 cells). Clinically active disease was defined as anterior chamber cells count grade $\geq+0.5$. Patients' data, including age, ethnicity, gender, and uveitis diagnosis, were collected at T0. Primary clinical features, including acute versus chronic, granulomatous versus non-granulomatous, infectious versus non-infectious, and anatomic location of uveitis, were determined clinically by the same examiner in each centre (FP and AI).

Clinical data, including best corrected visual acuity (BCVA) evaluated in LogMAR (logarithm of the minimum angle of resolution) and AC cells, were collected at each visit.

Additional investigations and management depended on underlying diagnosis, which was not changed based on this study.

2.2 | Imaging procedures

All patients underwent imaging with Spectralis® OCT (Heidelberg Engineering, Heidelberg, Germany) with

anterior segment module at T0, T1, and T2. All scans were performed by an experienced ophthalmic photographer and were supervised by the senior uveitis specialists in the two centres. Unlike OCT imaging of the posterior eye, gaze tracking and anatomical landmark registration are not currently possible during AS-OCT imaging with commercially available instruments. Therefore, participants were instructed to maintain steady fixation of the instrument's internal fixation target during image acquisition. The scan was retaken if an image was affected by a blink artefact or poor fixation.

After the anterior segment lens was placed and the patient positioned, the focus location was set to ±0.00 mm. A dense high-resolution 20° × 10° volume of 81 B-scans lines, each separated by 69 μm and consisting of 16 averaged B-scans, including 1024 A-scans, was chosen from the Cornea module and centred on the pupil. Averaging of the images (ART mean) and angle variation were used to ensure noise reduction and obtain crisp and detailed features of the identified KPs (Figure 1A).

Anterior segment photographs were taken in all cases at every time point with a canon 7D DSLR camera body attached to a Haag-Streit BX900 slit lamp to allow clinical correlation with AS-OCT findings.

2.3 | Image analysis

Rectangular volume scans, 11 mm-wide and 5.5 mm tall, made by 81 B-scans, were acquired from the lower hemisphere of the anterior segment using an anterior segment OCT device (Heidelberg Engineering, Heidelberg, Germany). Volumes were exported with the Heyex software (Heidelberg Engineering, Heidelberg, Germany) using the XML export function. Using this function, a folder was exported for each volume. The folder contained all B-scans, the infrared (IR) picture as '.tif' images, and a '.xml' file. The '.xml' file contained information about the order of the B-scans, their start- and end-position relative to the IR picture, and the axial/lateral resolution in micrometres. These data were used to segment the cornea boundaries and precipitates sequentially in all the B-scans of the volume. Then, segmentation results were used with the information from the '.xml' file to calculate the volume of precipitates per unit of analysed area, and to reconstruct a map of precipitates. All image processing operations were performed using MATLAB R2021b software (MathWorks, Natick, MA, USA) with the Image Processing Toolbox. All parameters and thresholds used were identified experimentally.

2.4 | Image segmentation

Images were processed sequentially, from the bottom to the top B-scan of a volume. The final segmentation was
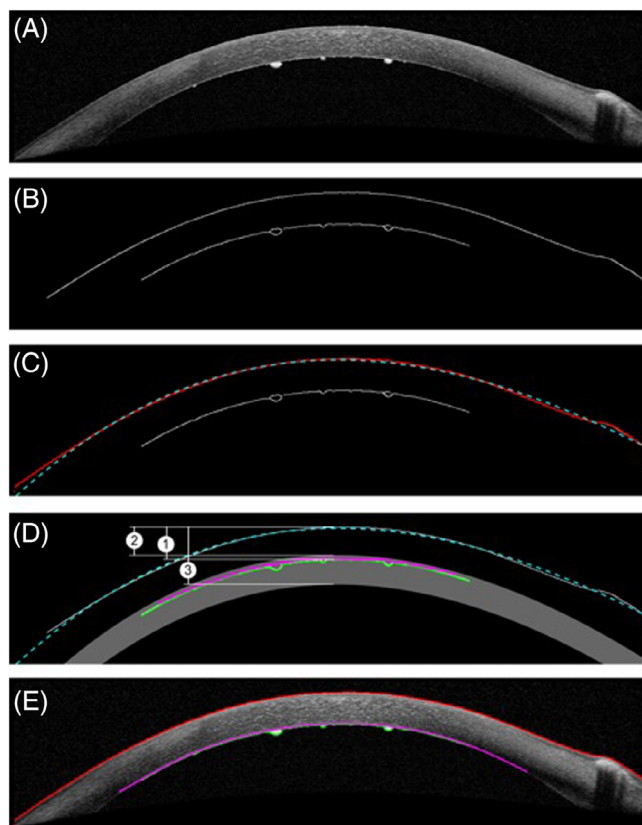

FIGURE 1 (A) A B-scan of the dataset. (B) The edges identified with the Canny method. (C) The edge-image and the segmented external boundary of the cornea in red, identified as the first edge from the top. The discontinued curve in cyan shows the curve c_{ext}, fitted to the segmented boundary. (D) The edge-image with the search area for the internal boundary, in grey. The search area is defined by the curve c_{ext} (discontinued cyan curve) and the estimated distance $d_{ext-int}$, marked with the number '1' in a white circle. The search area starts at a distance of $d_{ext-int} - 5$ pixels from c_{ext} (marked with the number '2') and ends at a distance of $d_{ext-int} + 40$ pixels from c_{ext} (marked with the number '3'). In green, are the lowest detected edge-points inside the search area. In magenta, is the convex profile of the lowest detected edge-points. (E) The final segmentation for the B-scan, with the external boundary of the cornea in red, the internal boundary of the cornea in magenta, and the profile of precipitates in green.

obtained through the sequential segmentations of the external boundary of the cornea, of the internal boundary of the cornea, and of precipitates.

2.4.1 | External boundary of the cornea

The external boundary of the cornea was identified as the first connected edge from the top of the B-scan from the edges identified by the Canny method (Figure 1C). For this operation, the 'edge' function provided by the Image Processing Toolbox (threshold = 0.6, sigma = 2) was used (Figure 1B). Then, a curve (c_{ext}) was fitted to

the boundary (Figure 1C). The curve was used to identify, remove, and replace possible outliers (points of the edge distant 20 pixels or more from the curve) with interpolated points. This operation was introduced to make the segmentation robust to artefacts in the scans, such as reflection artefacts that can often occur near the centre of the volume. The fitted curve c_{ext} was also used to define the search area for the segmentation of the internal boundary of the cornea.

2.4.2 | Internal boundary of the cornea

A search area for the edge of the internal boundary was obtained using c_{ext} and the estimated distance between internal and external boundaries ($d_{ext-int}$) of the cornea. The estimate $d_{ext-int}$ was calculated as the vertical difference between the highest point of the segmented, external boundary and the highest point of the longest edge below it, likely to belong to the inner edge. If no edge was identified inside the search area, the processing was halted, and the B-scan was excluded from the analysis. This was necessary to exclude B-scans not capturing the internal boundary, such as those at the bottom of the volume, where the cornea meets the iris. Using $d_{ext-int}$, the search area was defined as all the points at a distance between $d_{ext-int} - 5$ pixels and $d_{ext-int} + 40$ pixels below c_{ext} (Figure 1D). For each column in the search area, the lowest detected edge point was used to obtain a convex profile approximating the internal boundary (Figure 1D). Finally, a curve fitted on this profile was used as the initial guess for the active contour described in Ometto et al[14] to obtain the final segmentation (Figure 1E).

2.4.3 | Precipitates

The lowest edge points detected in the search area of the previous step were defined as the profile of precipitates. Every pixel between this profile and the internal boundary was assumed to belong to precipitates.

2.5 | Data processing

The analysis of segmentation results was limited to the top half of the B-scans. This restriction was introduced to ensure that measurements were not affected by the inclusion of structures near the cornea-iris junction, often imaged in the scans below this point. The position of the B-scans provided in the '.xml' file was used to identify the location of segmented structures relative to the IR image. Segmentation results were interpolated between successive B-scans to provide the exact resolution in both axes, reducing the effect of different B-scan spacings in

different acquisitions. These operations allowed the calculation of the volume of precipitates in mm^3 and the calculation of areas of the internal boundary of the cornea in mm^2. A ratio of the volume of precipitates over the analysed area was calculated for each volume. This ratio, in mm, could be interpreted as the elevation of precipitates if the measured precipitates-volume was spread equally over the analysed area. For each acquisition, this value provided a single measurement independent of the analysed area-size, allowing comparisons from different acquisitions. Finally, the interpolated results could be superimposed on the IR image using a colormap representing the elevation of the segmented precipitates (Figure 2).

2.6 | Statistical analysis

Where appropriate, descriptive statistics for continuous variables included the mean and standard deviation (SD). Differences in BCVA, clinically graded anterior chamber cells, and AS-OCT measurements of the KPs among the three groups were tested using a linear mixed model with the patient as a random effect.

Variations in the number of anterior chamber cells, AS-OCT measured KPs, and BCVA over time were assessed using a linear mixed model considering both the eye and the patient as random effects to account for repeated measurements within the same eye.

The influence of clinical variables, including visit, type of uveitis (infectious or non-infectious), was tested with linear mixed model, with the patient as a random effect.

The statistical analyses were run on the open-access R software (R Studio Version 1.1.383, R Project, www.r-project.org). p Values <0.05 were considered statistically significant. The Bonferroni correction was applied when multiple comparisons were performed.

3 | RESULTS

Twenty eyes from 20 patients were deemed eligible and included in the analysis. Of the 20 patients enrolled, 13 (65%) were females, and the mean (SD) age was 39 ($\pm$19) years. Eight patients (40%) suffered from PCR-confirmed infectious uveitis.

3.1 | Best corrected visual acuity

Average BCVA significantly improved from 0.77 ± 0.8 LogMAR units at T0 to 0.6 ± 0.5 LogMAR units at T2 ($p < 0.0001$), while the average anterior chamber cells count reduced from 2.1 ± 0.8 at T0 to 0.7 ± 0.8 at T2 ($p < 0.001$; Figure 3).

In the linear mixed model, BCVA was positively influenced by time ($p = 0.02$ from T0 to T1 $p = 0.0001$ and from T0 to T2) and negatively influenced by anterior chamber cells count. By contrast, BCVA was not affected by any other tested factors, including age, gender, and type of uveitis (infectious/non-infectious).

3.2 | KPs analysis

All patients underwent a complete ophthalmologic examination that revealed the presence of KPs in all affected eyes (Figure 4). Clinically, the KPs were stellate, medium-sized, and diffusely distributed on the entire posterior surface of the cornea in 11 eyes (55%); KPs were distributed in the inferior cornea in 9 eyes (45%).

At baseline, the mean [SD] volume of the corneal KPs was 0.1727 ± 0.072 mm^3. This figure was non-significantly reduced to 0.1511 ± 0.055 mm^3 ($p = 0.2$) at T1 and only significantly reduced to 0.1111 ± 0.038 mm^3 ($p = 0.03$) at T2 (Figure 3). This decreasing trend over time was seen in all eyes.

The ratio between the volume of the KPs in mm^3 and the corneal area in mm^2 progressively decreased from
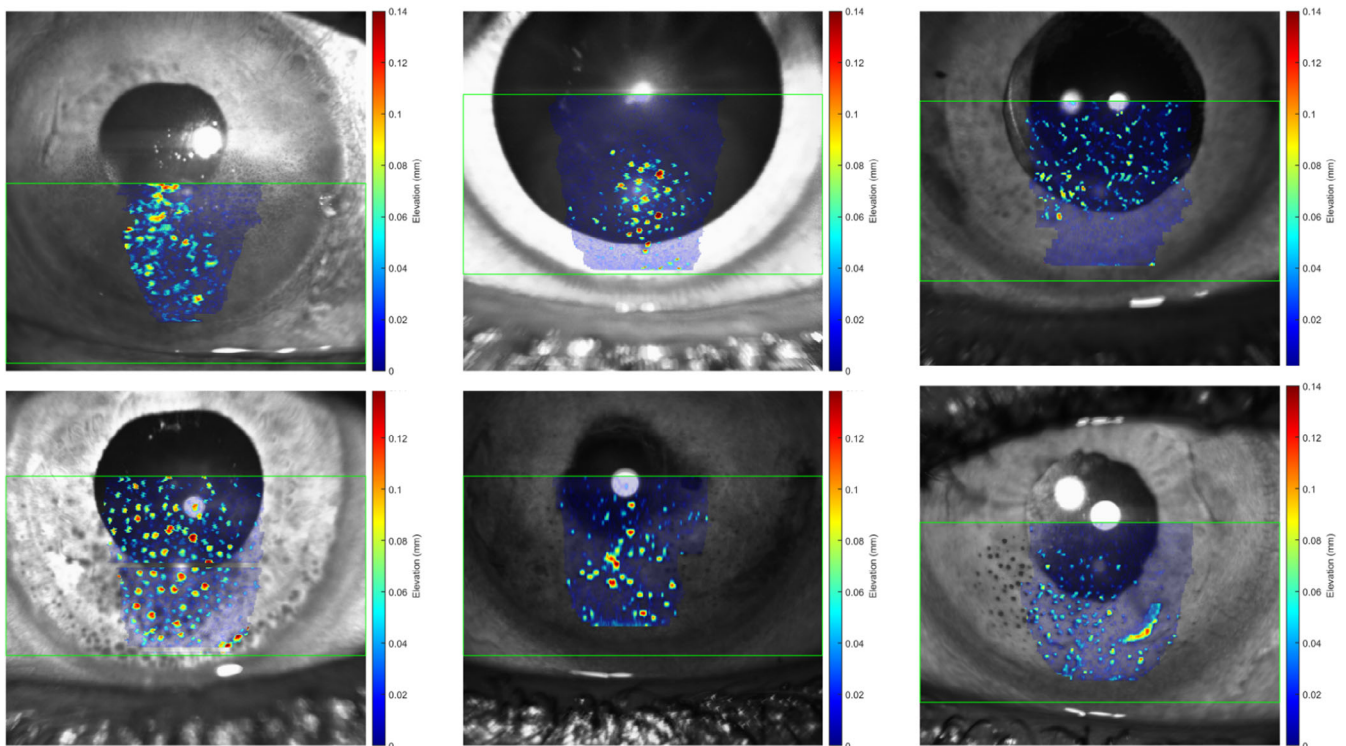

FIGURE 2 The infrared (IR) image, exported from the acquisition device, with a map of elevation of segmented precipitates superimposed. In translucent blue, is the analysed area. The green rectangle-box shows the location of the volume-acquisition, as reported in the '.xml' file.
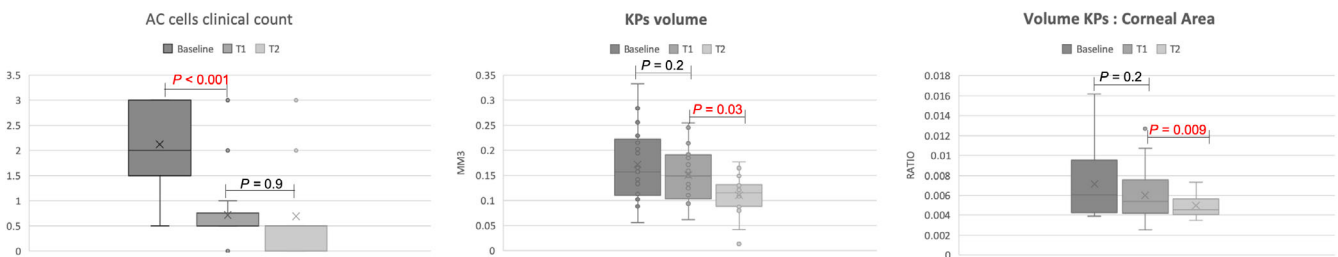

FIGURE 3 The average anterior chamber cells count of our cohort of 20 patients with uveitic keratic precipitates (KPs) reduced from 2.1 ± 0.8 at T0 to 0.7 ± 0.8 at T2 ($p < 0.001$; left panel). The mean volume of the corneal KPs was 0.1727 ± 0.072 mm^3 at T0, was non-significantly reduced to 0.1511 ± 0.055 mm^3 ($p = 0.2$) at T1 and only significantly reduced to 0.1111 ± 0.038 mm^3 ($p = 0.03$) at T2 (centre panel). The ratio between the volume of the KPs and the corneal area progressively decreased from T0 (0.007 ± 0.003) to T1 (0.006 ± 0.002; $p = 0.2$) and T2 (0.004 ± 0.001; $p = 0.009$; right panel).
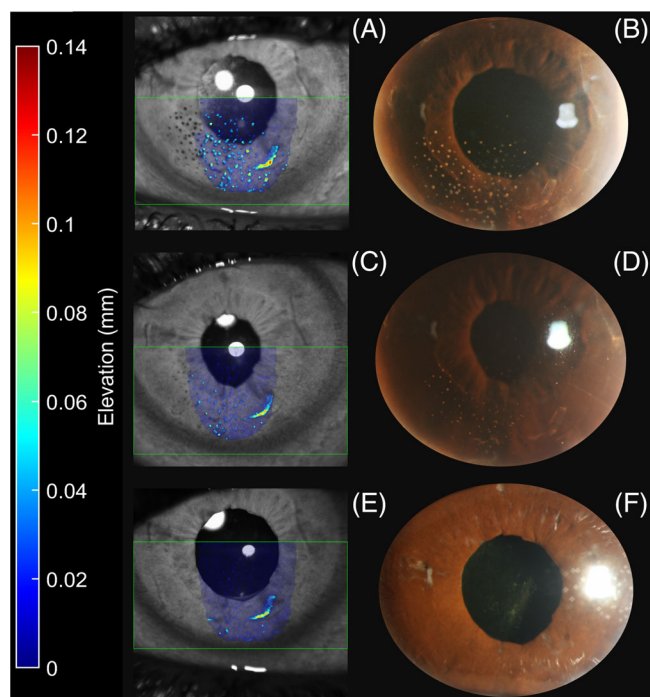
FIGURE 4 A patient with active uveitis and keratic precipitates (KPs) (B) at T0 and his corresponding en face rendering of the KPs (A) created through our algorithm. The colour-coded map shows the elevation of the KPs. With topical corticosteroid treatment, the anterior segment inflammation and the KPs improved at T1 as shown in the slit lamp photo (D) and this was reflected in the en face AS-OCT (C). A complete resolution of the inflammation was achieved at T2, both clinically (F) and in the objective KPs assessment (E).
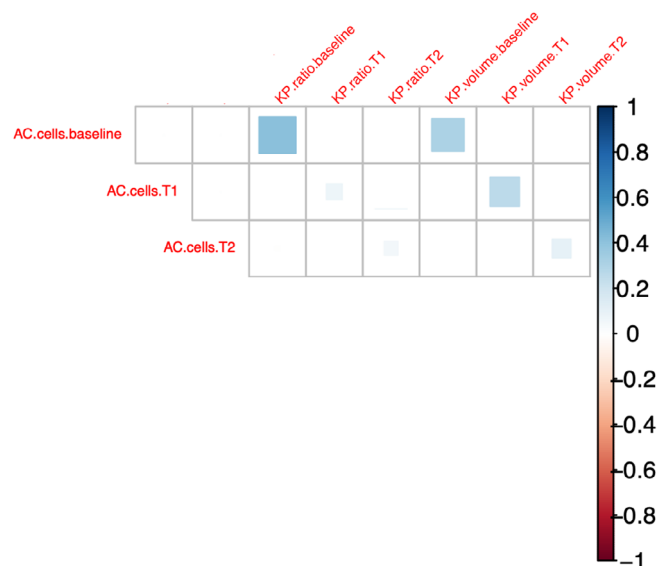

FIGURE 5 A plot showing the correlation between the clinical inflammatory parameters (AC cells) and the automated imaging keratic precipitates (KPs) measurements (KPs volume and KPS volume: area ratio) at the three time points (baseline, T1, and T2). There was a statistically significant correlation between the AC cell count and the AS-OCT volume measurements of the KPs at the three time points (red square). In contrast, the correlation between the volume: area ratio and the clinical assessment of inflammation did not reach significance.

T0 (0.007 ± 0.003) to T1 (0.006 ± 0.002; $p = 0.2$) and T2 (0.004 ± 0.001; $p = 0.009$), but the decrease was statistically significant only at T2 (Figure 3).

At T0, there was not a statistically significant difference between KPs secondary to infectious and non-infectious uveitis both in volume (0.1874 ± 0.086 vs. 0.1636 ± 0.064 mm^3, $p = 0.5114$) and in the ratio (0.006 ± 0.002 vs. 0.007 ± 0.004, $p = 0.7482$).

There was a statistically significant correlation between the AC cell count and the AS-OCT volume measurements of the KPs at the three time points (Figure 5). In contrast, the correlation between the volume: area ratio and the clinical assessment of inflammation did not reach significance (Figure 5).

4 | DISCUSSION

Over the past decade, significant efforts have been made to make the grading of intraocular inflammation more objective.[15] This current study introduces the use of automated software to accurately measure the areas of KPs, which could be a valuable addition.

Ever since the publication of the SUN grading system in 2005,[3] it has emerged as the widely accepted standard for reporting inflammation in different compartments of the eye in a standardised manner. However, several publications have pointed out certain limitations of this system, including its moderate agreement between different observers,[16] its inability to effectively distinguish lower levels of inflammation,[17] and its restricted application in clinical trial settings where a 2-point change must be considered significant.

Sharma et al[10] were the pioneers in utilising SD OCT-based scans of the anterior chamber to visualise cells as hyperreflective dots. They also employed automated software to calculate the number of cells per cubic millimetre, thereby establishing a continuous measure of inflammation that demonstrated a strong correlation with the clinical grading based on the SUN grading system. Invernizzi et al[9] replicated this study using SS-OCT scans of the anterior segment, albeit with the limitation of manually counting hyperreflective cells in the anterior chamber. Nevertheless, the Italian group was the first to objectively quantify anterior chamber haze by comparing the reflectivity of the anterior chamber (brighter in cases with a higher number of particles) with the air as an absolute intensity reference.

The process of standardising the measurement of vitreous haze through SD-OCT has evolved over time. Initially, it involved calculating the vitreous/RPE ratio[18] using ImageJ (http://imagej.net). Subsequently, it shifted to calculating the ratio between vitreous intensity and the mean values of the entire retina[19] to mitigate potential confounding effects of intensity signals caused by RPE disruption or shadowing from hyperreflective retinal structures.

In recent years, the application of SD-OCT for objective inflammation assessment has extended beyond the scope of the SUN grading scores. For instance, one parameter that the SUN Working Group excluded was vitreous cells, as they can be observed using a slit lamp. However, accurately determining the quantity of these cells remains a clinical challenge. Nevertheless, our group[20] has recently reported on manual and automated counting of hyperreflective oval particles as vitreous cells in patients with posterior uveitis, using SD-OCT scans.

KPs are among these 'orphaned' inflammatory signs that the SUN grading system has excluded.[3] However, the SUN workshop recognises the need for standardised descriptions of different types of KPs and the development of appropriate descriptive terms.

In vivo confocal microscopy (IVCM)[21–23] has been one of the initial imaging techniques used to study KPs from a morphological perspective. It has provided valuable insights into the heterogeneity of KPs that go beyond what can be observed with slit-lamp biomicroscopy. However, due to its limited utilisation in clinical practice and the scarcity of publications describing its application in imaging KPs, a consensus on the nomenclature for classifying KPs using IVCM is yet to be reached.

Wertheim et al[21] were the first to categorise KPs detected through IVCM into six main groups: globular, infiltrating, smooth-rounded, stippled, dendritiform, and cruciform. The authors speculated that the morphological features of KPs observed with IVCM might have consistent associations with specific disease states and could be diagnostically significant. Supporting this hypothesis, KPs in patients with active HLA-B27-associated uveitis have been described as stippled in multiple case series utilising IVCM.[21,22] However, subsequent studies have failed to establish a significant correlation between the morphological phenotypes observed with IVCM and the clinical classification of KPs as 'granulomatous' or 'non-granulomatous'.[22] Additionally, Kanavi et al[21] challenged Wertheim et al's initial theory[23] that infectious causes of KPs would display infiltrating and dendritic appearances. Kanavi et al found that in the majority of eyes with KPs showing such morphotypes, PCR analysis of aqueous specimens yielded negative results for the presence of common infectious agents associated with

uveitis.[21] This suggests that the presence of infiltrating and dendritiform KPs may not necessarily indicate an infectious aetiology.

Overall, studies utilising IVCM to examine KPs are hindered by the limited number of patients included in each clinical category. Additionally, their findings have had limited impact due to the low adoption of this imaging technique among clinicians.

SD-OCT, a second imaging modality utilised for examining the anterior segment, proves valuable in the investigation of KPs. In the pioneering work by Shipton et al,[13] 12-line radial scans (performed with the Topcon DRI OCT Triton Plus from Topcon, Japan) were employed, with each scan passing through the central cornea and selecting the clearest images displaying KPs. Various characteristics can be utilised to describe KPs on anterior segment OCT, such as their shape, border definition, size, and quantity. Shipton et al[13] utilised the Gnu Image Manipulation Program (GIMP) to analyse their reflectivity. Their findings suggested that hyperreflective KPs may indicate newly deposited KPs and active inflammation. However, no discernible differences in morphological appearance were found to distinguish between infective and non-infective aetiologies.

Our study is the second one to utilise AS-OCT for analysing KPs. Additionally, our objective goes beyond mere description, focusing not only on the morphology and reflectivity of KPs but also on creating an algorithm that converts the 81 SD-OCT volume lines into an en face OCT for calculating the baseline volume of KPs and their objective reduction with appropriate therapy.

The cohort consisted of 20 patients with uveitis of varying aetiologies. The study revealed an expected statistically significant decrease in anterior chamber cellularity (assessed subjectively via slit lamp) after just 1 month of therapy. Although the volume of KPs, as measured using our algorithm on SD-OCT scans, decreased from 0.1727 to 0.1511 mm^3 at 1 month, this reduction was not statistically significant. It was only after 2 months of therapy that the continuous decrease in KPs volume reached statistical significance (Figure 3).

Furthermore, we calculated a ratio of the volume of precipitates to the analysed area for each time point. This ratio serves as an indicator of precipitate elevation and allows for comparisons across different acquisitions, regardless of the size of the studied area. The volume-to-area ratio demonstrated a significant decrease at T2 compared to baseline (Figure 3).

The observed improvements in KPs volume and ratio at T2, albeit delayed compared to the decrease in AC cells, are expected. This delay is due to the fact that while cells in the anterior chamber consist of individual white blood cells that quickly resolve with therapy, KPs are

clusters of white blood cells and thus take longer to resolve.

Having established the possibility of objectively measuring KPs volume and its reduction over time with therapy using anterior segment OCT and our analysis algorithm, we then correlated the subjective cell count in the anterior chamber with the objectively obtained significance of precipitates through anterior segment OCT volume analysis. Our statistical analysis revealed a significant correlation between AC cells and KPs volume at the three different time points (Figure 5).

This opens up new potential applications for AS-OCT, where both anterior chamber cells and KPs can be evaluated through a single scan. This allows for the extraction of two numerical parameters and provides a comprehensive and objective assessment of anterior inflammation, thus eliminating the subjectivity between different clinicians' examinations.

The present study has several limitations. First, the sample size of the patients studied is small, and there is heterogeneity in terms of inflammatory pathologies, which reduces the intensity of the volumetric analysis of KPs of different types. Nonetheless, our research team aimed to validate the accuracy of anterior segment OCT in imaging inflammatory KPs and develop an algorithm capable of transforming the 81 lines of OCT data into a volumetric en face image within a few minutes. To achieve this goal and demonstrate the correlation between objectively measured KP volumes and subjectively assessed inflammation (using standardised measures), we considered 20 eyes to be a suitable starting point. Additionally, it is important to note that uveitic pathologies with KPs are rare and should not be overlooked.

Another limitation of the study pertains to the scanning pattern that was employed. Based on the assumption that the majority of KPs are situated in the lower half or third of the cornea, we opted to conduct scans using 81 lines spanning from the centre of the pupil to the lower limbus. As a result, some precipitates located above the scanned area were inevitably excluded. This limitation can be addressed in future research endeavours by implementing a raster of SD-OCT lines to scan the entire cornea, which can then be transformed into a comprehensive en face image of the entire corneal surface using the pre-existing algorithm.

The methodology's limitation was observed in restricting the analysis solely to the top half of the B-scans, which consequently restricted the overall area under analysis. Although expanding the analysis to cover the entire scan could enhance the algorithm, it may also introduce potential measurement errors. The excluded areas of the scan, specifically the bottom corners, are often characterised by weaker signals, making them more susceptible to inaccurate measurements. This limitation could be addressed in the future by including just a percentage of the central cornea, so as to ensure that the area of analysis does not vary.

Finally, patients with a known diagnosis of corneal ectasia were excluded, and further study correlating automated AS-OCT detection of the corneal boundaries with corneal topography and elevation map of the posterior cornea may be needed to further validate our algorithm.

In summary, our current study successfully showcased the capability of anterior segment OCT in imaging uveitic KPs. To achieve this, we developed a customised algorithm that converted OCT scans into en face renderings, enabling us to accurately estimate the volume of KPs and provide an objective quantification of these inflammatory changes. Notably, we observed a significant correlation between the objective quantification of KPs and the counts of inflammatory cells in the anterior chamber, implying a potential application of this parameter in the evaluation and monitoring of intraocular inflammation. Our findings serve as an initial step towards future investigations involving larger sample sizes, aiming to validate the clinical feasibility of analysing KPs through AS-OCT. This could lead to an in-built OCT software for fast analysis of ocular inflammation, and it could project uveitis into the world of virtual reviews (telemedicine), which are well established in certain parts of the world in glaucoma, macular degeneration, and diabetes.

CONFLICT OF INTEREST STATEMENT
The authors declare no conflict of interest.

DATA AVAILABILITY STATEMENT
The data that support the findings of this study are available on request from the corresponding author. The data are not publicly available due to privacy or ethical restrictions.

ORCID
Francesco Pichi https://orcid.org/0000-0002-7357-4166
Alessandro Invernizzi https://orcid.org/0000-0003-3400-1987

REFERENCES
1. Chan NS, Chee SP. Keratic precipitates: the underutilized diagnostic clue. *Ocul Immunol Inflamm.* 2021;29(4):776-785.
2. Goldstein DA, Tessler HH. Classification, symptoms, and signs of uveitis. In: Tasman W, Jaeger EA, eds. *Duane's Clinical Ophthalmology.* Vol 4. Lippincott Williams & Wilkins; 2004.

3. Jabs DA, Nussenblatt RB, Rosenbaum JT, Standardization of Uveitis Nomenclature (SUN) Working Group. Standardization of uveitis nomenclature for reporting clinical data. Results of the first international workshop. *Am J Ophthalmol.* 2005;140: 509-516.

4. Yanoff M, Fine BS. *Basic Principles of Pathology.* 5th ed. Mosby; 2002.

5. Tandon R, Sihota R. *Text Book of Parson's Diseases of Eye.* Elsevier Health Sciences; 2014.

6. Rathinam SR, Babu M. Algorithmic approach in the diagnosis of uveitis. *Indian J Ophthalmol.* 2013;61:255-262.

7. Izatt J, Hee MR, Swanson EA, et al. Micrometer-scale resolution imaging of the anterior eye in vivo with optical coherence tomography. *Arch Ophthalmol.* 1994;112(12):1584-1589.

8. Jancevski M, Foster C. Anterior segment optical coherence tomography. *Semin Ophthalmol.* 2010;25(5–6):317-323.

9. Invernizzi A, Marchi S, Aldigeri R, et al. Objective quantification of anterior chamber inflammation: measuring cells and flare by anterior segment optical coherence tomography. *Ophthalmology.* 2017;124(11):1670-1677.

10. Sharma S, Lowder CY, Vasanji A, Baynes K, Kaiser PK, Srivastava SK. Automated analysis of anterior chamber inflammation by spectral-domain optical coherence tomography. *Ophthalmology.* 2015;122(7):1464-1470.

11. Invernizzi A, Cigada M, Savoldi L, Cavuto S, Fontana L, Cimino L. In vivo analysis of the iris thickness by spectral domain optical coherence tomography. *Br J Ophthalmol.* 2014; 98(9):1245-1249.

12. Zarei M, Mahmoudi T, Riazi-Esfahani H, et al. Automated measurement of iris surface smoothness using anterior segment optical coherence tomography. *Sci Rep.* 2021;11(1):8505.

13. Shipton C, Hind J, Biagi J, Lyall D. Anterior segment optical coherence tomographic characterisation of keratic precipitates. *Cont Lens Anterior Eye.* 2020;43(5):465-468.

14. Ometto G, Moghul I, Montesano G, et al. ReLayer: a free, online tool for extracting retinal thickness from cross-platform OCT images. *Transl Vis Sci Technol.* 2019;29(3):25.

15. Denniston AK, Keane PA, Srivastava SK. Biomarkers and surrogate endpoints in uveitis: the impact of quantitative imaging. *Invest Ophthalmol Vis Sci.* 2017;58(6):BIO131-BIO140.

16. Jabs DA, Dick A, Doucette JT, et al. Standardization of uveitis nomenclature working group. Interobserver agreement among uveitis experts on Uveitic diagnoses: the standardization of uveitis nomenclature experience. *Am J Ophthalmol.* 2018;186: 19-24.

17. Khairallah M. Are the Standardization of the Uveitis Nomenclature (SUN) Working Group criteria for codifying the site of inflammation appropriate for all uveitis problems? Limitations of the SUN Working Group classification. *Ocul Immunol Inflamm.* 2010;18(1):2-4.

18. Keane PA, Karampelas M, Sim DA, et al. Objective measurement of vitreous inflammation using optical coherence tomography. *Ophthalmology.* 2014;121(9):1706-1714.

19. Barbosa J, Syeda S, Rodriguez-Torres Y, Le K, Lin X. Quantifying vitreous inflammation in uveitis: an optical coherence tomography prospective study. *Can J Ophthalmol.* 2020;55(5): 352-358.

20. Zicarelli F, Ometto G, Montesano G, et al. Objective quantification of posterior segment inflammation: measuring vitreous cells and haze using optical coherence tomography. *Am J Ophthalmol.* 2023;245:134-144.

21. Wertheim MS, Mathers WD, Planck SJ, et al. In vivo confocal microscopy of keratic precipitates. *Arch Ophthalmol.* 2004; 122(12):1773-1781.

22. Kanavi MR, Soheilian M, Naghshgar N. Confocal scan of keratic precipitates in uveitic eyes of various etiologies. *Cornea.* 2010;29(6):650-654.

23. Kanavi MR, Soheilian M, Yazdani S, Peyman GA. Confocal scan features of keratic precipitates in Fuchs heterochromic iridocyclitis. *Cornea.* 2010;29(1):39-42.